Computational Investigation of Blast-wave-mitigation via the Use of Air-vacated Buffers

M. Grujicic, J. S. Snipes, N. Chandrasekharan

Department of Mechanical Engineering

Clemson University

Clemson, SC, 29634, USA

gmica@clemson.edu

Abstract

Several experimental investigations reported in the open literature have indicated that the application of reduced pressures of air (within a closed vessel) carrying detonation-induced blast waves can substantially reduce the intensity of blast loading experienced by the target test-structure (placed inside the vessel). To examine the feasibility and potential of this air-vacation concept in protecting target structure/personnel under more realistic combat-theatre conditions, the use of air-vacated buffers placed in front of the target structure is investigated in the present work. Towards that end, advanced fluid-structure interaction, non-linear dynamics, finite-element analyses are carried out on the phenomena and processes accompanying blast wave generation, propagation and interaction with air/buffer and buffer/target-structure interfaces. To verify and validate the employed computational methods and tools, it was first shown that they can quite accurately reproduce analytical solutions for a couple of well-defined blast wave propagation and interaction problems. To quantify the blast/mitigation efficiency of the air-vacated buffer concept, two metrics are utilized: (a) the peak pressure experienced by the target structure; and (b) the total momentum/impulse transferred by the incident blast wave to the target structure. The results obtained clearly revealed that significant blast-mitigation effects can be achieved through the use of the air-vacated buffer concept and that the extent of the blast-mitigation effect is a sensitive function of the buffer geometrical and vacated-air material-state parameters (e.g., pressure, mass density, etc.). It has also been shown that, in order to fully exploit the air-vacated buffer concept, timely deployment of the buffer is very critical.

Keywords

Blast-wave-mitigation; Air-vacation; Computational Analysis

Introduction

The main objective of the present work is to utilize advanced fluid-structure interaction computational methods and tools in order to assess the blast-mitigation potential of air-vacated buffers placed between the incident blast wave(s) and the target structure/personnel. Hence, the key aspects of the present work are: (a) blast-wave-loading; (b) shock/blast-wave-mitigation strategies/concepts; and (c) use of air-vacated buffers in blast-wave-mitigation applications. These aspects will be briefly overviewed in the remainder of this section. It should be noted that the term "blast wave" is used here to denote a high-intensity detonation-induced wave within the air surrounding the explosive charge, while the term "shock" is used to denote the high intensity wave within the target structure generated as a result of the interaction of the incident blast wave with the target structure.

Blast-wave-loading: Blast waves are high intensity waves which propagate through a fluid medium (e.g. air) and after collision with target structures exert time-dependent loading on to the structures, transferring to them substantial momentum and kinetic energy. Blast waves are generally produced as a result of intentional or accidental explosions. In the combat theatre, explosions are normally intentional and result from the detonation of various explosives. In the civilian/industrial environment, on the other hand, explosions are often the result of accidents or negligence. Regardless of the circumstances under which explosions occur, there is a general need to develop blast-resistant structures which could protect infrastructure and personnel. Development of such structures is generally costly, time consuming and involves destructive (one-shot) testing. Consequently, in order to shorten the time and reduce the cost of such development, full-scale testing is increasingly being complemented (and often replaced) with subscale testing and computational engineering analyses (CEA) [1-5]. In the present work, advanced CEA methods and tools are used in the analysis of an air-vacated buffer based blast-wave-mitigation strategy.

Blast waves analyzed in the present work are the result of the detonation of an explosive charge. Detonation is a process which rapidly (i.e. at a rate governed by the speed of blast waves within the explosive charge) converts condensed explosive material into a high-pressure/high-density/high-temperature, rapidly-expanding mass of gaseous detonation-products. High-rate expansion of the gaseous detonation products into the surrounding air produces outward-propagating air-borne blast waves (of a spherical shape, in the case of free-air detonation, and a hemispherical shape in the case of ground detonation). Unlike the (smooth/continuous) sound/acoustic waves, blast waves produce discontinuous changes in the material state variables (i.e. pressure, mass density, temperature, etc.) across the wave front. Fig. 1(a) shows a prototypical pressure vs. time trace at a fixed point relative to the free-air explosive-detonation location. Examination of Fig. 1(a) reveals that at the time of arrival, t_a, of the blast wave at a given point of interest, pressure experiences an abrupt change from its initial/ambient value, p_0, to a peak value, p_s, (p_s - p_0 is commonly called the "peak over-pressure"). Thereafter, the pressure decreases and, at a post-detonation time of $t_a + t_d$ (t_d is commonly called the positive phase duration and is on the order of a few tens of microseconds), becomes equal to the ambient pressure, p_0. Subsequently, within the so-called "suction-phase", the pressure first continues to drop at a progressively lower rate, reaches a minimum and then begins to asymptotically approach the ambient pressure level.

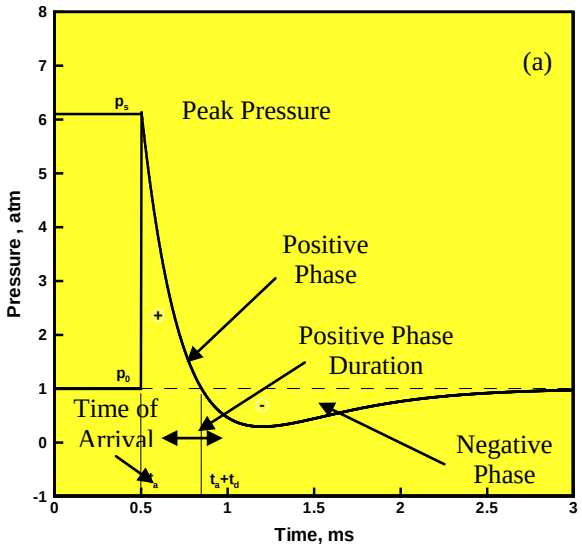

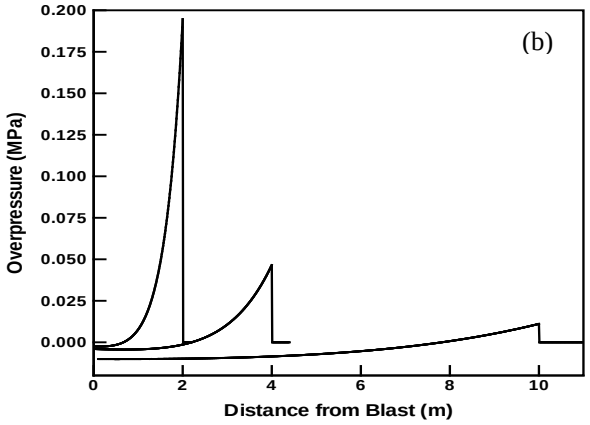

FIGURE 1 (a) A TYPICAL FREE-AIR PRESSURE VS. TIME RELATION AT A FIXED POINT AS DEFINED BY THE BIPHASIC FRIEDLANDER EQUATION; AND (b) RADIAL DISTRIBUTION OF THE BLAST-INDUCED OVERPRESSURE ASSOCIATED WITH 1KG TNT DETONATION AT POST-DETONATION TIMES OF 1.9MS, 6.4MS AND 22.7MS

The air-borne blast-wave pressure profile depicted in Fig. 1(a) is usually represented using the biphasic Friedlander functional relation [6] as:

$$p(t) = (p_s - p_0)e^{-(t-t_a)/\tau}\left[1 - \frac{t-t_a}{t_d}\right] + p_0;\ t >= t_a \qquad (1)$$

$$p(t) = p_0;\ otherwise$$

where τ is a time constant which controls both the rate of pressure decrease from its p_s value and the lowest pressure attained during the suction phase.

When analyzing the interaction of the air-borne blast wave with a solid structure, one should be cognizant of the fact that there are two components ($p_r(t) - p_0$ and $p_i(t) - p_0$) of the blast-induced overpressure, $p(t)$ - p_0 and that both of these components are defined by the functional relation given in (1). Parameters t_a and t_d are identical for the two components of pressure while the remaining two parameters p_s and τ generally differ in the two cases. For a general case of a solid surface whose outward normal makes an angle θ with a vector connecting the surface section to the explosive charge centroid, the total pressure experienced by the target surface is given as:

$$p(t) = p_i(t)[1 + \cos\theta - 2\cos^2\theta] + p_r(t)\cos^2\theta,\ \cos\theta > 0 \qquad (2a)$$

$$p(t) = p_i(t),\ \cos\theta \le 0 \qquad (2b)$$

Examination of (2a) reveals that in the case of a target surface which is tangential to the spherically

expanding blast wave ($\cos\theta$ = 1), only the reflected component of the pressure (p_r) is present. On the other hand, in the case of a target surface that is along one of the radial directions ($\cos\theta$ = 0), only the incident pressure component, p_i, is present.

Due to the fact that, when a blast wave strikes the target surface (at a zero obliquity angle) the gas molecules are abruptly brought to rest, (conservation of linear momentum demands that) $p_r - p_0$ is higher than $p_i - p_0$. The associated overpressure magnification factor $(p_r - p_0)/(p_i - p_0)$ is typically around 2.0 in the case of weak blast waves. Overpressure magnification factors as high as 8.0 and 20.0 have been reported in the case of stronger blast waves in ideal gases and non-ideal gases, respectively [7].

While the plot shown in Fig. 1(a) depicts temporal evolution of the pressure at a fixed stand-off distance (a radial distance from the charge center of mass), it is often useful to show radial distribution of pressure as a function of the post-detonation time. An example of the latter plot is depicted in Fig. 1(b) for the case of 1kg TNT at the post-detonation times (1.9ms, 6.4ms and 22.7ms) corresponding to the blast wave arrival at the radial locations 2m, 4m and 10m from the charge center of mass. It is seen that as the (spherically-shaped) blast wave expands, it undergoes attenuation and dispersion/spreading.

In the absence of experimental results, the bi-phasic Friedlander blast-wave pressure-profile parameters like p_s-p_0, t_a, t_d and τ are often predicted using CONWEP, an empirically-based blast simulation code developed by the US Army Corps of Engineers [8]. Within CONWEP [8], all the incident and reflected pressure parameters used in (1) are assumed to be functions of a scaled distance (defined as a ratio of (i) the distance between the loaded surface and the explosive charge centroid, and (ii) a cube root of the TNT equivalent explosive charge mass). In addition, t_a, t_d and are proportional to the cube root of the charge mass. It should be noted that the results displayed in Fig. 1(b) were obtained using CONWEP.

Shock/Blast-Wave-Mitigation Strategies/Concepts: Since blast-wave loading can generally cause substantial damage and destruction of the target structure and severe injury or fatality of the targeted personnel, various shock-mitigation strategies and concepts have been investigated over the last several decades. Whereas it is not the intention of the present work to provide a comprehensive overview of all shock-mitigation concepts, it appears that they could be generally classified (on the basis of the physical phenomena and processes employed) as: (a) strategies based on the dissipation of the energy carried by the shocks induced in blast-wave impacted structures. An example of this type of strategy can be found in the case of polyurea blast-mitigating coatings, in which shock-wave energy dissipation is accomplished through activation of a second-order rubbery-to-glassy phase transition under shock-loading [9, 10]; (b) strategies based on the absorption of the energy carried by the shocks induced in blast-wave impacted structures. An example of this type of strategy can be found in the case of the foam-filled protective structures, in which shock-induced foam densification acts as a potent energy absorbing mechanism [11]; (c) strategies based on the attenuation and dispersion of the energy carried by the shocks induced in blast-wave impacted structures. An example of this type of strategy can be found in the case of granular-material based protective structures [12]; (d) fluid-structure interaction strategies based on the reduction in the momentum transfer from the blast wave to the target structure, which result in weaker shocks within the structure. An example of this type of strategy can be found in structurally optimized metallic sandwich plates in which strike-face mass is reduced (relative to the honeycomb-core mass) in order to reduce momentum ingress into the structure [13]; and (e) strategies based on the shock impedance mismatch, whose main goal is again to reduce momentum ingress into the structure. An example of this type of strategy is the use of air-vacated buffers (the subject of the present work) [14].

Use of Air-Vacated Buffers in Blast-Wave-Mitigation Applications: Examination of the blast-mitigation strategies presented above reveals that those falling into groups (a) – (c) deal with shocks within the target structure, while strategies in group (d) deal with the interaction of the incident blast waves with the target structure. In contrast, the air-vacated buffer strategy, falling into group (e), deals with the medium through which the incident shock propagates before interacting with the target structure and aims at reducing the intensity of the incident blast wave. Specifically, to reduce the intensity of the incident blast wave, an air-vacated buffer region is placed in front of the targeted structure.

Examination of the public-domain literature identified several studies in which the concept of air-vacation was investigated, experimentally and/or

computationally. For example, in [15] free-plate blast loading was carried out within an air-filled and evacuated spherical tank, and the effect of air evacuation on reducing the intensity of blast-loading was clearly demonstrated. Similar findings were reported in [16], but in the case of a tank partially filled with vermiculite. In the studies reported in [15, 16] air-vacation was employed within the entire space of propagation of the incident blast waves. Clearly, attainment of such conditions is not practical (or, generally, not even feasible) and, within the present work, a case was considered within which air-vacation is employed (using a finite-thickness buffer only in the region adjacent to the target structure). The mechanism by which such an air-vacated buffer can lower the intensity of the incident blast waves will be discussed in greater detail in the next section.

Main Objective: As mentioned earlier, the main objective of the present work is to employ state-of-the-art fluid-structure interaction computational methods and tools in order to assess blast-mitigation potential of air-vacated buffers placed between the incident blast wave(s) and the target structure/personnel. In meeting this objective, it was found critical to establish validity of the employed computational methods and tools. This was done by comparing the numerical results yielded by these methods/tools with their analytical counterparts for a couple of relatively simple blast-wave propagation/interaction problems for which the analytical solutions were known.

Organization of the Paper: Details regarding the definition of the problems at hand, formulation of the corresponding mathematical models and the transient, non-linear dynamics, explicit finite-element analysis used are presented in Section II. The procedure used to validate the employed computational methods and tools, as well as the associated computational results, are described in Section III. The results pertaining to the predicted blast-mitigation efficiency of the air-vacated buffer concept are presented and discussed in Section IV. The main conclusions resulting from the present work are summarized in Section V.

Problem Definition and Computational Analysis

The basic problem analyzed in the present work involves generation, propagation and interaction of detonation-induced blast waves with an air-vacated buffer and/or a rigid immobile structure. While the problem at hand is of a three-dimensional character (and possesses spherical symmetry, in the case of free-air explosion and hemispherical symmetry, in the case of ground-laid explosive-charge detonation) it is treated, in the present work, as being of a one-dimensional nature. The reason for this simplification is that the main objective of the present work is to establish the potential for air-vacation buffer based blast-wave-mitigation, and not to obtain a highly accurate assessment of this potential in specific explosive-charge-detonation scenarios. Since the problem analyzed in the present work involves the interaction of blast waves propagating within air with a solid structure, a new Combined Eulerian Lagrangian (CEL) fluid-structure interaction (FSI) computational analysis is employed. Within this analysis, the complete formulation of the mathematical model for the problem at hand involves specification of the following aspects of the problem: (a) geometrical and meshed model(s); (b) initial conditions; (c) boundary conditions; (d) fluid-structure interactions; (e) material model(s); (f) computational analysis type; (g) computational algorithm; and (h) computational accuracy, stability and cost.

Geometrical and Meshed Model(s): The (Eulerian) computational domain is of a high-aspect ratio, rectangular parallelepiped shape with its longest edge aligned in the x_1-direction (the direction of propagation of a planar, longitudinal blast wave, being analyzed). A schematic of the computational domain used is shown in Fig. 2(a). Since the (incident) blast wave propagates in the positive x_1-direction and ultimately interacts with a rigid immobile surface, the Lagrangian portion of the computational domain coincides with the right-most face (orthogonal to the x_1-direction of the Eulerian domain), Fig. 2(a).

The (Eulerian) computational domain is discretized using first-order, hexahedron, eight-node Eulerian elements, as shown in Fig. 2(b). As seen in this figure, the number of these elements in the x_2- and x_3-directions is one. The reason for this simplification is that the mesh model shown in Fig. 2(b) is used to analyze one-dimensional behavior of the planar, longitudinal blast wave and, hence, the computational cell dimensions and the number of elements in the lateral directions are immaterial. For the same reason, the very low aspect ratio of the finite elements used is

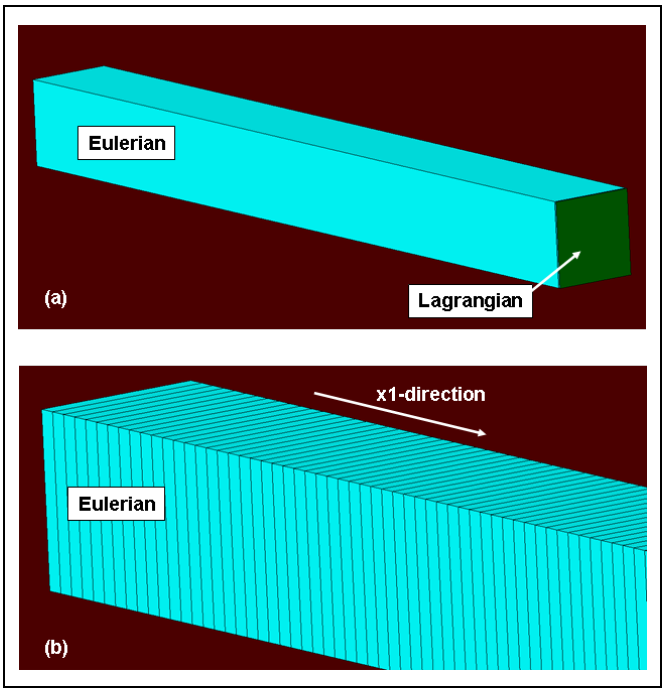

FIGURE 2 TYPICAL: (a) GEOMETRICAL; AND (b) MESHED MODELS USED IN THE PRESENT WORK. PLEASE NOTE THAT, FOR CLARITY, ONLY A PORTION OF THE MESHED MODEL IS SHOWN

of no concern. As far as the Lagrangian domain is concerned, it is meshed as a single four-node shell element.

Initial Conditions: At the beginning of each simulation, the Eulerian domain is filled with air. As far as the static pressure, temperature and particle velocities are concerned, their initial values are set in accordance with the problem being analyzed. Essentially, two classes of problems were analyzed: (a) the propagation and interaction of fully-supported blast waves (the term "fully-supported" will be defined later); and (b) the propagation and interaction of decaying blast waves (to be defined later).

In the case of fully-supported blast waves, shock-jump equations are used to compute the pressure, temperature and particle velocity in the (left-most) portion of the computational domain swept by the blast wave (prior to the beginning of the simulation). Pressure and temperature in the air in front of the fully-supported forward-travelling blast wave are set equal to their ambient-air counterparts, while the particle velocity is set to zero. In addition, in the cases in which an air-vacated buffer is present, the portion of the Eulerian region adjacent to the rigid, immobile surface (located at the far-right section of the computational domain) is assigned a low pressure, ambient temperature and zero particle velocity. Fig. 3(a) is constructed in order to help clarify the initial conditions used in the fully-supported blast wave case.

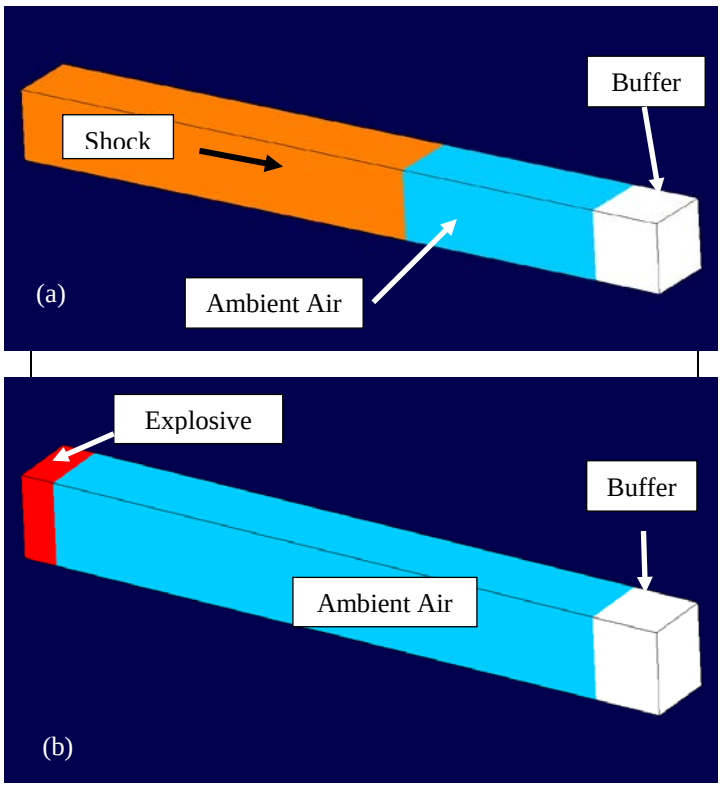

FIGURE 3 INITIAL CONDITIONS USED IN DIFFERENT PORTIONS OF THE EULERIAN DOMAIN WITHIN THE ANALYSES DEALING WITH: (a) FULLY-SUPPORTED BLAST WAVES; AND (b) DETONATION-INDUCED DECAYING BLAST WAVES

In the case of decaying blast waves, the explosive-charge energy is used to compute the pressure and temperature (particle velocity is set to zero) in the (left-most) portion of the computational domain initially containing the explosive charge. Pressure and temperature in the air in front of the exploded-charge region are again set equal to their ambient-air counterparts, while the particle velocity is set to zero. In addition, in the cases in which an air-vacated buffer is present, the portion of the Eulerian region adjacent to the rigid, immobile surface is again assigned a low pressure, ambient temperature and zero particle velocity. Fig. 3(b) is constructed in order to help clarify the initial conditions used in the decaying blast wave case.

Boundary Conditions: To account for the one-dimensional character of the problem at hand and for the longitudinal character of the (incident) blast waves, "no-flow" boundary conditions are applied along the domain faces orthogonal to the x_2- and x_3-directions. Furthermore, to comply with the rigid, immobile surface condition employed in the present analysis, fluid-structure interaction/contact boundary conditions are applied along the right-most face of the Eulerian

domain, while "fixed" boundary conditions are applied to the Lagrangian domain. As far as the boundary conditions applied along the left-most face of the Eulerian domain are concerned, they differed between the two types of problems analyzed. That is, in the case of the fully-supported blast waves, "in-flow" boundary conditions are used with a constant particle velocity equal to that predicted by the shock-jump equations. On the other hand, in the decaying blast wave case, symmetry-type boundary conditions are used.

Fluid-Structure Interactions: Since the Eulerian and Lagrangian domains possess conformal meshes, the contact interfaces between the two are defined using mesh-based surfaces. Eulerian-Lagrangian interaction/contact constraints are enforced using a penalty method, within which the extent of contact pressure is governed by the local surface penetrations (where the default penalty stiffness parameter is automatically maximized subject to stability limits). Due to the longitudinal character of the blast waves travelling within the Eulerian domain, no generation or transmission of the shear stresses had to be considered. Also, due to the presence of a single material (air) within the Eulerian domain, no interactions between different Eulerian materials had to be accounted for.

Material Model(s): As mentioned earlier, the Eulerian domain is filled solely with air (i.e. gaseous detonation products are treated as air). Air is modeled using an ideal gas equation of state (an equation which relates the material static pressure with its mass density and temperature or the internal energy density). Details regarding the ideal gas equation of state (EOS) will be presented in the next section. Since air is considered to be of a zero shear-stiffness and inviscid (of a zero viscosity), it cannot support/develop any shear stresses. Hence, no shear-stress constitutive relation(s) had to be defined.

As far as the Lagrangian domain is concerned, it is treated as a rigid immobile structure and, hence, no definition of a material model is required.

Computational Analysis Type: The problem at hand is analyzed computationally using a Combined Eulerian Lagrangian, fluid-structure interaction, finite-element algorithm. Within this algorithm, the Eulerian mesh is fixed spatially while the Eulerian material(s) is allowed to flow through it. At the same time, the Lagrangian mesh is attached to (and moves with) the Lagrangian material. Since the Lagrangian material is rigid and immobile, in the present case, the Lagrangian mesh also remains stationary during the simulation.

Computational Algorithm: Numerical solution of the governing equations in the Eulerian sub-domain within each time increment involves two separate steps: (a) the Lagrangian step within which the sub-domain is temporarily treated as being of a Lagrangian-type (i.e. Eulerian-mesh nodes and elements are attached to and move/deform with the Eulerian material); and (b) the "remap" step within which the distorted Eulerian mesh is mapped onto the original Eulerian mesh and the accompanying Eulerian material transport is computed and used to update the Eulerian-material states and inter-material boundaries.

The problem is solved using an explicit solution algorithm implemented in ABAQUS/Explicit, a general purpose finite element solver [17].

Computational Accuracy, Stability and Cost: In order to ensure that the results obtained are accurate, (i.e. insensitive to further refinement in the elements' size), a standard mesh sensitivity analysis was carried out (the results not shown for brevity).

Due to the conditionally-stable nature of the explicit finite element analysis used, the maximum time increment during each computational step had to be lower than the attendant stable time increment. The use of a time increment smaller than the stable time-increment ensures that neither a blast wave nor the Eulerian material travels a distance (within a given time increment) which is longer than the element's shortest dimension.

Regarding the computational cost, due to the quite simple nature of the geometrical and mesh models used, it was not of a major concern. A typical computational analysis carried out in the present work using a 12 core, 3.0GHz machine with 16GB of memory required less than five minutes of wall-clock time.

Validation of the Fluid-structure Interaction Code

As mentioned earlier, in all the calculations carried out in the present work, ABAQUS/Explicit, a commercial transient non-linear dynamics explicit finite-element code [17], was used. In this section, a couple of simple blast-wave-propagation/blast-wave-interaction problems, for which analytical/closed-form solutions exist, are investigated using this computational tool. The main purpose of this investigation was to validate the tool and assess the extent of its computational

accuracy. The two problems analyzed in this section both involve propagation of planar, longitudinal, compressive, fully-supported blast waves within ambient, quiescent (zero particle velocity) air. The term "fully-supported" used here, denotes the condition(s) when the state of the material behind the blast wave (as represented by static pressure, material mass density, particle velocity, etc.) is constant (i.e. does not decay with distance from the blast wave front). In the first problem, the blast wave interacts with a rigid, immobile planar surface and reflects as a stronger blast wave propagating in a direction opposite to that of the incident blast wave. In the second problem, the same incident blast wave interacts with an air-vacated buffer (separated from the incident- blast wave bearing air by a planar interface) and produces a transmitted blast wave into the buffer (travelling in the same direction as the incident blast wave) and a backward-travelling centered simple release wave (the concept of a centered simple wave will be defined later.).

Blast-wave Reflection from a Rigid Immobile Surface

The interaction of a planar, longitudinal, compressive, fully-supported blast wave, propagating within the ambient quiescent air, with a rigid, immobile planar interface is a well understood problem. As schematically shown in Figs. 4(a)-(b), the interaction in question produces a backward-travelling reflected blast wave which is stronger than the forward-travelling incident blast wave. The corresponding time vs. position plot is depicted in Fig. 4(c). In this figure, two horizontal lines are used to denote the respective times associated with the blast wave positions shown in Figs. 4(a)-(b).

When the ideal-gas type Equation of State (EOS) is used for air and a constant specific-heat ratio, $\gamma=C_p/C_v$ (C_p and C_v are, respectively, the constant-pressure and constant-volume specific heats), is assumed, then the reflected blast wave characteristics can be readily computed. Specifically, the reflection coefficient, C_R, defined as the ratio of the reflected-blast wave overpressure, $p_r - p_0$, and the incident-blast wave overpressure, p_s-p_0, can be defined in terms of the specific heat ratio and the incident-blast wave overpressure as:

$$C_R = \frac{p_r - p_0}{p_s - p_0} = \frac{(3\gamma - 1)\frac{p_s - p_0}{p_0} + 4\gamma}{(\gamma - 1)\frac{p_s - p_0}{p_0} + 2\gamma} \qquad (3)$$

where p_0, p_s, p_r, are respectively the ambient air, incident-blast wave and reflected- blast wave (absolute) static/side-on pressures.

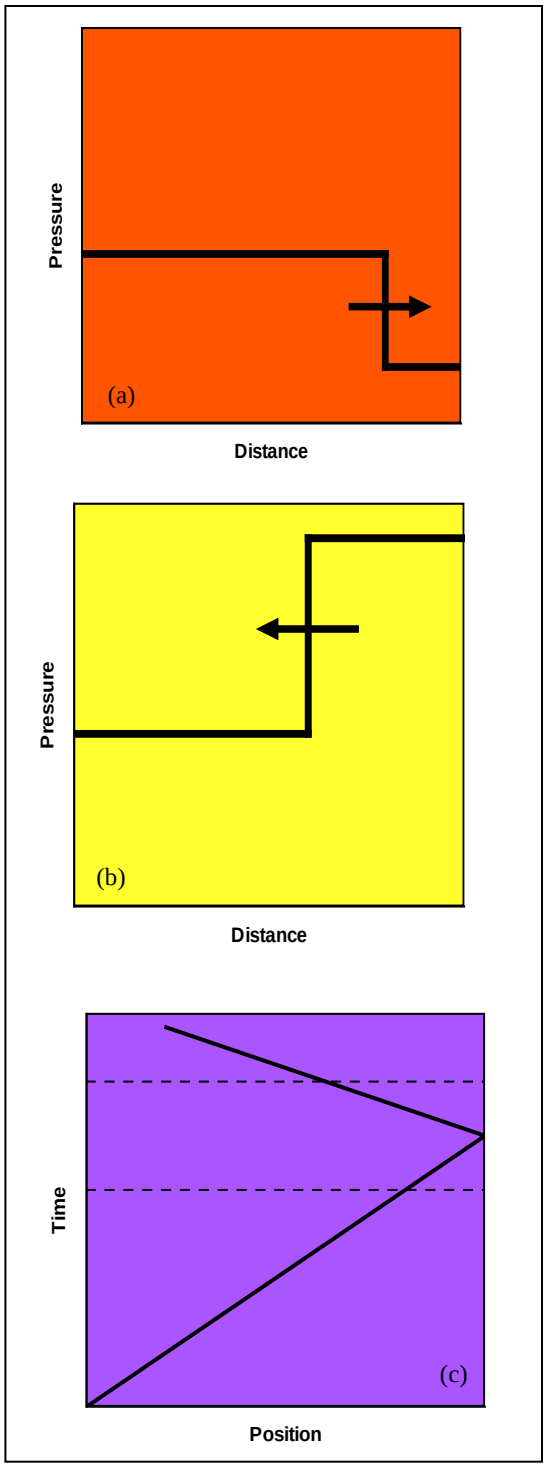

FIGURE 4 INTERACTION OF A FULLY-SUPPORTED PLANAR LONGITUDINAL BLAST WAVE (PROPAGATING, TO THE RIGHT, WITHIN THE AMBIENT AIR) WITH A PLANAR, RIGID, IMMOBILE TARGET STRUCTURE: (a) AND (b) DENOTE POSITIONS OF THE BLAST-WAVE FRONT AT TWO DIFFERENT TIMES (THE TARGET STRUCTURE IS LOCATED AT THE FAR RIGHT); AND (c) SHOWS TIME VS. BLAST-WAVE FRONT POSITION AND THE ASSOCIATED MATERIAL STATES IN FRONT OF AND BEHIND THE BLAST-WAVE FRONT

For the same case, the ratio of the material mass density behind the reflected blast wave, ρ_r, and that in the ambient air, ρ_0, can also be defined using the constant specific heat ratio and the incident-blast wave overpressure as:

$$\frac{\rho_r}{\rho_0} = \frac{\gamma\frac{p_s - p_0}{p_0} + \gamma \quad (\gamma+1)\frac{p_s - p_0}{p_0} + 2\gamma}{(\gamma-1)\frac{p_s - p_0}{p_0} + \gamma \quad (\gamma-1)\frac{p_s - p_0}{p_0} + 2\gamma} \quad (4)$$

The ABAQUS/Explicit validation procedure employed in this portion of the work involved a numerical determination of the reflection coefficient and the density ratio as a function of the incident-blast wave overpressure, and a comparison of the numerical results with their analytical counterparts as predicted by (3), (4) respectively. The results of this validation effort are shown in Figs. 5(a)-(b). In Fig. 5(a), C_R is plotted as a function of p_s-p_0 , while in Fig. 5(b), ρ_r/ρ_0 is depicted as a function of the same incident-blast wave overpressure. Examination of the results shown in these figures suggests that the fluid-structure interaction computational algorithm implemented in ABAQUS/Explicit reproduces the analytical results quite accurately. In fact, the largest errors observed are on the order of 0.1% for both the reflection coefficient and the density ratio.

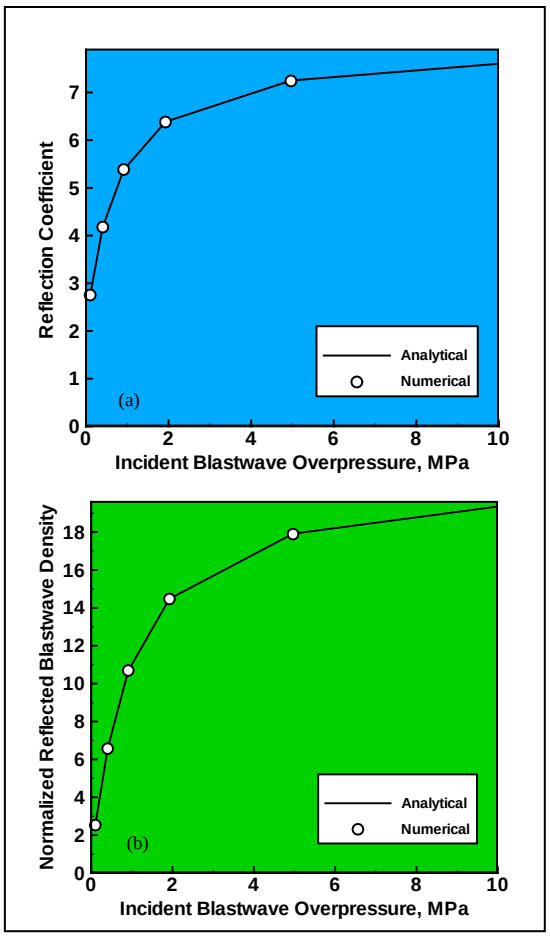

FIGURE 5 VALIDATION OF THE NUMERICAL CODE USED THROUGH THE CALCULATION OF: (a) THE REFLECTION COEFFICIENT; AND (b) THE NORMALIZED REFLECTED BLAST-WAVE DENSITY RATIO FOR THE CASE OF A FULLY-SUPPORTED PLANAR LONGITUDINAL BLAST WAVE (PROPAGATING, TO THE RIGHT, WITHIN THE AMBIENT AIR AND) IMPACTING A PLANAR, RIGID, IMMOBILE TARGET STRUCTURE

Blast-wave Interaction with Air/Buffer Interface

The interaction of a planar, longitudinal, compressive, fully-supported blast wave, propagating within the ambient, quiescent air, with an air/buffer planar interface is also a well understood problem. As schematically shown in Figs. 6(a)-(b), the interaction in question produces a forward-travelling blast wave within the buffer (which is weaker than the forward-travelling incident blast wave) and a backward-travelling centered, simple release/decompression wave. In addition, the air/buffer interface is imparted forward motion. As shown in Fig. 6(b), pressure remains constant across the air/buffer interface. The same can be said for the particle velocities. However, other material state variables (e.g. mass density, internal-energy density, temperature, etc.) experience a discontinuous change at this interface. Consequently, the air/buffer interface acts as a contact discontinuity which will interact with any incoming blast wave.

As far as the release wave is concerned, it is characterized here as being of a "centered, simple" nature. The term "simple" refers to the fact that the wave advances into the material of a constant state (i.e. into the constant material state produced by the incident blast wave). The term "centered" implies that all the characteristics/wavelets of the wave emanate from the same point in the time vs. spatial coordinate domain (i.e. the point in time at which the incident blast wave arrives at the air/buffer interface), Fig. 6(c). Since the release wave is of a continuous type (i.e. not a material-state discontinuity) its propagation is governed by the mass, linear momentum and energy conservation equations. A simple analysis of the energy conservation equation reveals that this equation stipulates that the wave propagation causes only isentropic changes in the material through which the waves propagate. Then the remaining two (mass and momentum) conservation equations, within the spatial/Eulerian frame are defined as:

$$\rho_t + u\rho_x + \rho u_x = 0,$$
$$u_t + uu_x + \frac{p_x}{\rho} = 0 \quad (5)$$

and

$$p = f(\rho),$$
$$a^2 = f'(\rho). \quad (6)$$

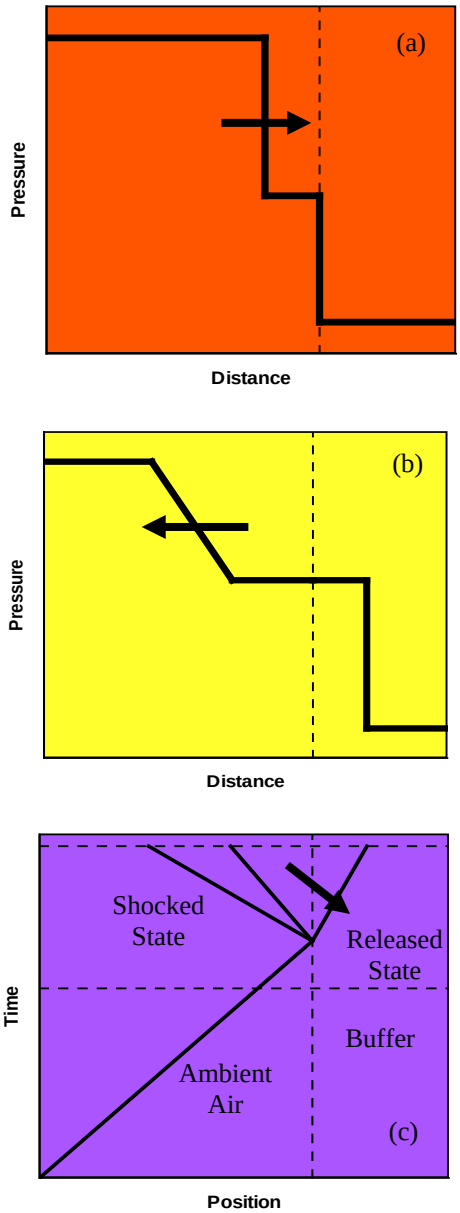

FIGURE 6. INTERACTION OF A FULLY-SUPPORTED PLANAR LONGITUDINAL RIGHT-PROPAGATING BLAST WAVE WITH A PLANAR, AMBIENT-AIR/BUFFER INTERFACE: (a) AND (b) DENOTE POSITIONS OF THE BLAST WAVE FRONT AND RELEASE WAVE LEADING AND TRAILING CHARACTERISTICS AT TWO DIFFERENT TIMES (THE AMBIENT-AIR/BUFFER INTERFACE IS DENOTED BY THE VERTICAL DASHED LINE); AND (c) SHOWS TIME VS. BLAST-WAVE FRONT/RELEASE WAVE-SPREAD POSITION AND THE ASSOCIATED MATERIAL STATES SEPARATED BY THESE WAVES

where subscripts t and x denote, respectively, partial derivatives with respect to the time and (single) spatial coordinate, while u, ρ and p represent, respectively, the particle velocity, mass density and static pressure. The speed of sound, a, for air (modeled as an ideal gas) is defined as:

$$a = \sqrt{\frac{\gamma p}{\rho}} \quad (7)$$

For a simple wave, (5), (7) can be solved using the method of characteristic variables [18]. Characteristic variables are unique independent variables (obtained by combining t and x) which, when used in (5), (6) enable decoupling of these equations. Obtaining the solution to these equations then becomes a quite straightforward procedure. In the case of a centered, simple wave, there is only one characteristic variable, and the lines associated with a constant value of the characteristic variable (the "characteristics") are all straight and emanate from the same point in the t vs. x plot, Fig. 6(c). The solution to (5), (6) for a backward-travelling centered, simple wave (of interest in the present work), can be summarized as follows:

$$u - a = \text{characteristic - dependent constant} \quad (8)$$

$$\frac{u}{2} + \frac{a}{\gamma - 1} = \text{constant everywhere in the } t, x \text{ space} \quad (9)$$

Since the material state (u, ρ,, p and a) ahead of the backward-propagating release wave is known (i.e. defined by u_s, ρ_s, p_s and a_s), one can evaluate the constant appearing in (9). Since the same equation also applies to the material swept by the release wave (as defined by u_1, $\rho_{1,air}$, p_1 and $a_{1,air}$), evaluated (9) defines the first relationship between the unknown material states (u_1, $\rho_{1,air}$, p_1). Note that (a) subscript, air is used to denote a quantity at the air side of the air/buffer interface; and (b) a, as indicated by (7), should not be counted as a separate dependent variable.

The second condition relating the material states swept by the release wave arises from the isentropic condition and can be defined as:

$$\frac{p_1}{p_s} = \left(\frac{\rho_{1,air}}{\rho_s} \right)^{\gamma} \quad (10)$$

To obtain the third equation relating the material states swept by the release wave, one must invoke the condition for pressure and particle-velocity continuity

across the air/buffer interface. In other words, one must take into account that the pressure and the particle velocity in the air, swept by the release wave, are equal to their respective counterparts in the buffer, swept by the transmitted blast wave. To do this, one must add shock-jump equations, (i.e. equations defining material state discontinuities across the transmitted blast-wave front) to the present analysis.

For mathematical convenience, the mass, linear momentum, and energy shock-jump equations are generally defined with respect to a moving frame, i.e. a frame which is attached to the (transmitted, in the present case) blast-wave front. These equations can then be stated as:

$$\rho_v u_v' = \rho_{1,buffer} u_2' \quad (11)$$

$$p_v + (\rho_v u_v')^2 = p_1 + (\rho_{1,buffer} u_1')^2 \quad (12)$$

$$\rho_v u_v' \left(e_v + \frac{p_v}{\rho_v} + \frac{(u_v')^2}{2}\right) = \rho_{1,buffer} u_1' \left(e_{1,buffer} + \frac{p_1}{\rho_{1,buffer}} + \frac{(u_1')^2}{2}\right) \quad (13)$$

where primed particle velocities are defined with respect to the moving frame as $u_v' = u_v - U_s$ and $u_1' = u_1 - U_s$, where U_s is the transmitted blast wave velocity and subscript v is used to denote the initial material state within the buffer.

Examination of (11), (13) reveals that these equations introduce three additional dependent variables: (i) $\rho_{1,buffer}$; (ii) $e_{1,buffer}$; and (iii)U_s. Thus, the overall equation system indeterminacy remains. However, the ideal-gas EOS applied to the material state behind the transmitted blast wave:

$$p_1 = (\gamma - 1)\rho_{1,buffer} e_{1,buffer} \quad (14)$$

introduces no additional variables and makes the system determinate.

Mathematical manipulation of (9)-(14) can be used to derive the following expressions:

$$\frac{p_s}{p_v} = \frac{p_1}{p_v}\left[1 + \frac{\gamma - 1}{2a_s}\left(u_s - \frac{a_v}{\gamma}\frac{\frac{p_1}{p_v} - 1}{\sqrt{\frac{\gamma+1}{2\gamma}\left(\frac{p_1}{p_v} - 1\right) + 1}}\right)\right]^{\frac{2\gamma}{1-\gamma}} \quad (15)$$

$$u_1 = u_s + \frac{2a_s}{\gamma - 1}\left(1 - \left(\frac{p_1}{p_s}\right)^{\frac{\gamma-1}{2\gamma}}\right) \quad (16)$$

Eqs. (15-16) enable computation of p_1 and u_1 as a function of the incident blast-wave overpressure, $p_s - p_0$, and the buffer pressure, p_v. Within this section, the ABAQUS/Explicit code is validated by numerically reproducing the analytical results predicted by (15), (16). The results of this validation effort are shown in Figs. 7(a)-(b). In Fig. 7(a), p_1 is plotted as a function of p_s-p_0, while in Fig. 7(b), u_1 is depicted as a function of the same incident-blast wave overpressure. In both cases, the buffer pressure was kept constant and equal to 1.013 kPa (0.01 atm). Examination of the results shown in these figures suggests that the fluid-structure interaction computational algorithm implemented in ABAQUS/Explicit reproduces the

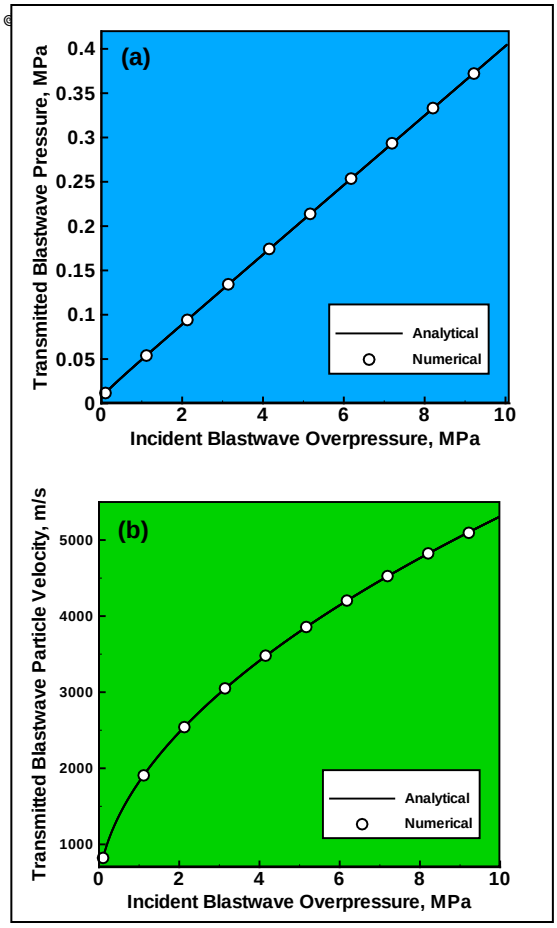

FIGURE 7 VALIDATION OF THE NUMERICAL CODE USED THROUGH THE CALCULATION OF: (a) THE TRANSMITTED BLAST WAVE PRESSURE; AND (b) THE TRANSMITTED BLAST WAVE PARTICLE VELOCITY FOR THE CASE OF A FULLY-SUPPORTED PLANAR LONGITUDINAL BLAST WAVE (PROPAGATING, TO THE RIGHT, WITHIN THE AMBIENT AIR AND) INTERACTING WITH A PLANAR AMBIENT-AIR/BUFFER INTERFACE

analytical results quite accurately. In fact, the largest errors observed are on the order of 0.1% for both p_1 and u_1.

Blast-wave Interaction with an Air-vacated Buffer

Now that the ABAQUS/Explicit code is validated, the attention is focused onto the problem of interaction of an incident (decaying) blast wave with an air-vacated buffer and the subsequent interaction of the transmitted blast wave with the target structure. Two distinct types of analyses are carried out: (a) within the first one, contact interactions between the buffer and the surrounding air are enabled only after the moment of incident blast wave arrival at the air/buffer interface; and (b) within the second case, the same contact interactions are activated before the incident blast wave arrives at the air/buffer interface. As will be discussed below, separate analyses of these two scenarios are critical in properly assessing the blast-wave-mitigation potential of the air-vacated buffer concept.

It should be noted that in the computational analyses carried out within the present section, the process of explosive charge detonation is not modeled explicitly (since this process is associated with a timescale several orders of magnitude smaller than the analyses timescale). Instead, explosive charge detonation is assumed to create, at $t = 0$, a high pressure, high density, high temperature region (of a size comparable to that of the explosive charge) containing gaseous detonation products. The material state within the exploded charge region is then typically specified using one of the two following approaches:

(a) the "isothermal-sphere" approach within which the (spherically-shaped) explosive charge energy and radius along with the detonation products' constant temperature are specified. Then, from the ideal-gas EOS given by (14) and its alternative form, $p = \rho RT$ (R is the known air-gas constant), one can determine the corresponding p and ρ values ; and

(b) the "point-source" approach within which the explosive charge is shrunken to a point and only the explosion-charge total energy has to be specified. Then, under an "ideal-explosion assumption" (i.e. under a condition that the ambient pressure is so small in comparison to the detonation pressure that it could be neglected), the similarity property of the point-source solution can be taken advantage of in order to compute distribution of the material states in the vicinity of the point-source. Due to a rapid decrease in the detonation pressure with time, the ideal-explosion assumption is valid only over a very short post-detonation time. Once the point-source solution is computed at a properly-selected short post-detonation time, it could be used as an initial condition in the subsequent blast wave buffer analysis.

In the work carried out in the present section, both of these blast-initialization approaches were utilized and the key results obtained were found to be quite comparable. Hence, only the results obtained using the isothermal-sphere blast-initialization approach will be presented and discussed in the present section.

Case without Air-vacated Buffer

Before presenting the results obtained in the analyses in which an air-vacated buffer is used, a few results

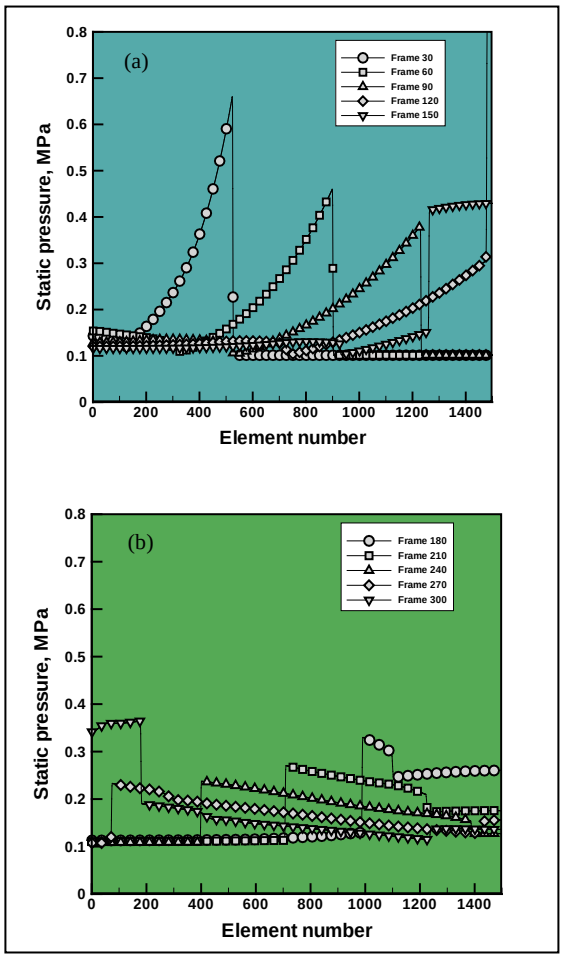

FIGURE 8. SPATIAL DISTRIBUTION OF THE DECAYING BLAST WAVE THROUGHOUT THE EULERIAN DOMAIN AS A FUNCTION OF THE POST-DETONATION TIME (QUANTIFIED BY THE ANIMATION- FRAME NUMBER) IN THE CASE WHEN NO AIR-VACATED BUFFER IS USED. THE FIGURE IS SEPARATED INTO PARTS (A) AND (B) TO IMPROVE CLARITY

will be shown and discussed for the case in which no buffer is employed. Examples of the results obtained in this case are displayed in Figs. 8(a)-(b) and 9(a)-(b). In Figs. 8(a)-(b), spatial distribution of the pressure throughout the Eulerian domain is plotted at ten different post-detonation times (denoted by the corresponding animation-frame number). In Figs. 9(a)-(b), on the other hand, time evolution of the pressure in two Eulerian elements (one located near the explosive charge, at the far left, and the other in contact with the rigid, immobile target, at the far right) is shown. Examination of the results displayed in Figs. 8(a)-(b) reveals that: (a) detonation produces a decaying forward travelling (incident) blast wave. (Compare the results corresponding to Frames 30, 60, 90 and 120); (b) reflection of the incident blast wave from the rigid-immobile structure creates (around Frame 120) a reflected, backward propagating blast wave and subjects the target structure to a relatively high pressure (this point will be discussed in greater detail below); (c) between Frames 90 and 120, a secondary forward-propagating blast wave is created. Formation of the secondary incident blast wave is related to the oscillatory nature of the pressure in the region behind the blast-wave front. That is, the pressure in this region drops sharply and then recovers quite quickly creating the conditions for the formation of the secondary incident blast wave. It should be noted that the pressure in the region surrounding and including the detonation site remains higher than the ambient-air pressure. This finding is consistent with the fact that the Eulerian domain analyzed is closed and hence, the final equilibrium pressure in this domain will be higher than the ambient-pressure; (d) the reflected and the secondary incident blast wave intersects between Frames 150 and 180; and (e) the secondary incident blast wave impacts the target structure at a time between Frames 240 and 270. This impact further increases the contact pressure experienced by the target structure.

Examination of the results displayed in Figs. 9(a)-(b) reveals that: (a) in the element adjacent to the detonation site, the pressure builds up quickly and then, equally as quickly, decreases to a value below the ambient air pressure and gradually recovers. At a later time, the pressure within this element experiences an abrupt increase (from 0.1072 MPa to 0.4516 MPa) due to the arrival of the backward-travelling, reflected blast wave (Fig. 9a) ; (b) pressure experienced by the Eulerian element neighboring the target structure remains at the ambient-air level (0.1013 MPa) until the

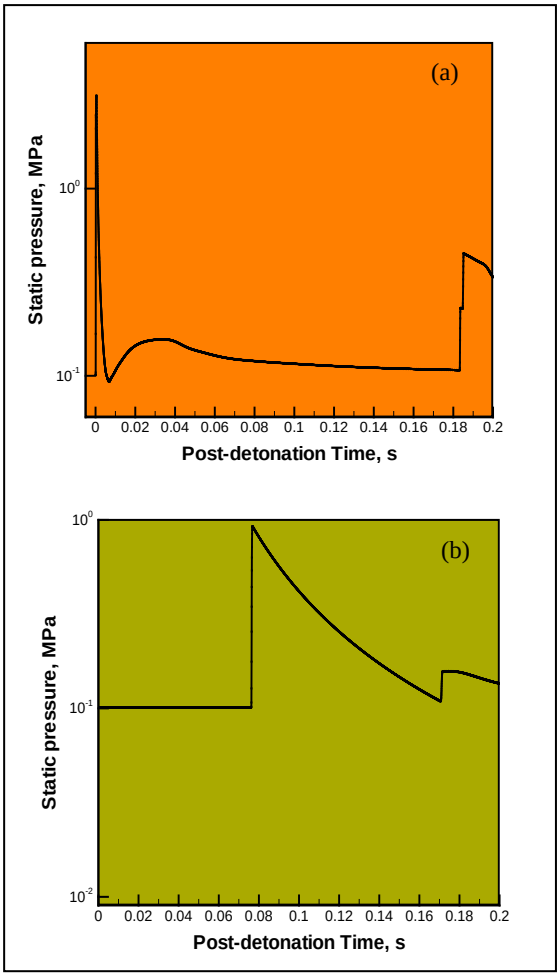

FIGURE 9. TEMPORAL EVOLUTION OF THE STATIC PRESSURE IN: (a) AN ELEMENT LOCATED NEAR THE EXPLOSIVE CHARGE; AND (b) AN ELEMENT ADJACENT TO THE RIGID, IMMOBILE TARGET STRUCTURE IN THE CASE WHEN NO AIR-VACATED BUFFER IS USED

arrival of the (primary) forward-propagating incident blast wave at which point the pressure increases to a value of 0.9238 MPa; and (c) the pressure in the same element then decreases exponentially until the arrival of the secondary incident wave, at which point an abrupt increase in the contact pressure (from 0.1092 MPa to 0.1618 MPa) experienced by the target takes place. It should be noted that, in the present analysis, the contact pressure experienced by the target is equal to the static pressure in the adjacent Eulerian element and, hence, the two quantities can be used interchangeably.

Timely Deployment of the Air-vacated Buffer

In the case presented in this section, a virtual partition is placed between the ambient air and the buffer and this partition is removed at the instant of arrival of the incident blast wave to the ambient-air/buffer interface. Consequently, no interaction takes place between

ambient air and the buffer. Rather, the incident blast wave interacts directly with the buffer. This condition ensures a maximum blast-wave-mitigation effect offered by the air-vacated buffer concept.

Typical results obtained in this portion of the work are displayed in Figs. 10(a)-(b) and 11(a)-(b). In Figs. 10(a)-(b), spatial distribution of the static pressure through the Eulerian region at different post-detonation times are shown. In Figs. 11(a)-(b), temporal evolution of the static pressure is depicted for the same two elements defined earlier in conjunction with Figs. 9(a)-(b), i.e. for an element located near the explosive charge (at the far left of the Eulerian domain), and for another element in contact with the rigid, immobile target (at the far right of the domain).

Examination of the results displayed in Figs. 10(a)-(b) reveals that: (a) detonation-induced decaying forward-travelling (incident) blast wave reaches the ambient-air/buffer interface at a time between Frames 90 and 100; (b) at Frame 120, it is seen that the transmitted forward-travelling blast wave within the buffer (resulting from the interaction of the incident blast wave with the buffer) has reflected from the rigid, immobile structure. This subjects the target structure to a peak pressure of 0.6132 MPa. This represents roughly a 30% reduction in this quantity relative to its value in the aforementioned case when no buffer was used; (c) arrival of the primary incident blast wave to the ambient-air/buffer interface also produces a backward-travelling release wave. However, due to a high strength of the primary incident blast wave and the associated high values of the (forward-travelling) particle velocity, the release wave, within the Eulerian frame, is carried in the forward direction ; (d) at Frame 150, it is seen that the backward-travelling reflected blast wave has substantially attenuated the release wave; (e) by Frame 180, the backward-travelling reflected blast wave has completely annihilated (and has been substantially attenuated by) the release wave, and it has intersected with the previously-mentioned secondary incident blast wave; and (f) the secondary incident blast wave impacts the target structure at a time between Frames 240 and 270. This impact increases the contact pressure (from 0.1227 MPa to 0.1522 MPa) experienced by the target structure.

Examination of the results displayed in Figs. 11(a)-(b) reveals that: (a) temporal evolution of the pressure within the element adjacent to the detonation site (identified in conjunction with Fig. 9(a)) is quite similar to that observed in the no-buffer case, Fig. 9(a). In fact, the only significant differences occur at times after the arrival of the reflected backward-travelling blast wave. This arrival causes an abrupt increase in pressure from 0.1068 MPa to 0.3931 MPa. A comparison of these results with their no-buffer case counterparts reveals that the pressure jump in question is reduced through the use of the buffer by ca. 12%.

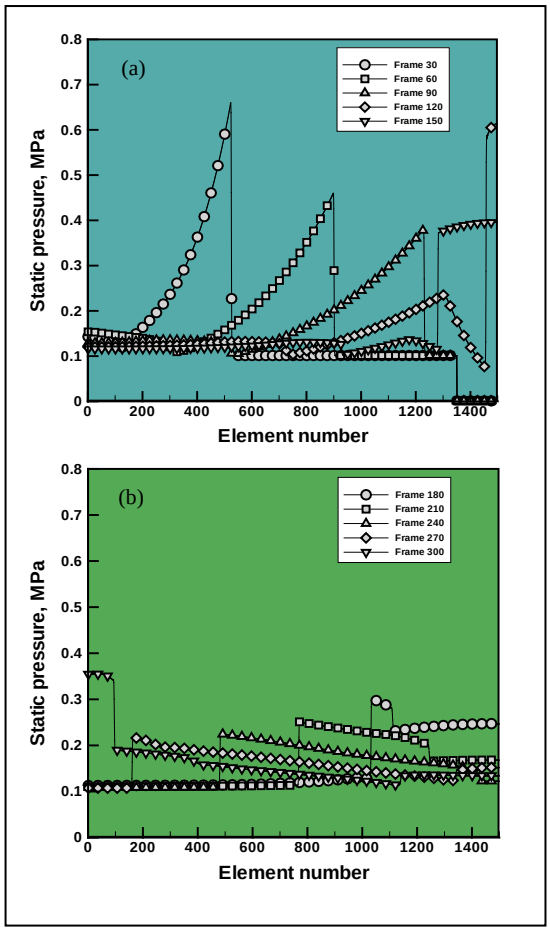

FIGURE 10. SPATIAL DISTRIBUTION OF THE DECAYING BLAST WAVE THROUGHOUT THE EULERIAN DOMAIN AS A FUNCTION OF THE POST-DETONATION TIME (QUANTIFIED BY THE ANIMATION- FRAME NUMBER) IN THE CASE WHEN AN AIR-VACATED BUFFER IS USED AND THE BUFFER IS ACTIVATED AT THE TIME OF ARRIVAL OF THE BLAST WAVE AT THE AMBIENT-AIR/BUFFER INTERFACE. THE FIGURE IS SEPARATED INTO PARTS (a) AND (b) TO IMPROVE CLARITY

This finding is consistent with the fact that the incident wave impacting the target structure (and, hence, the reflected blast wave) is stronger in the no-buffer case ; (b) pressure experienced by the Eulerian element neighboring the target structure remains at the buffer pressure level (0.0010 MPa) until the arrival of the transmitted forward-propagating blast wave at which point the pressure increases to a value of 0.6133 MPa; (c) the pressure in the same element first decreases and then recovers and stays high for a short period. This behavior is caused by the fact that the first reflected

backward-travelling blast wave within the buffer reflects from the contact discontinuity between (what used to be) ambient air and the buffer. This process generates a new forward-travelling blast wave which, upon impact, further loads the target structure and leads to the formation of yet another reflected blast wave. This whole sequence of events repeats until the contact discontinuity arrives at the buffer/structure interface; and (d) the pressure in the same element then decreases exponentially until the arrival of the secondary incident wave, at which point an abrupt increase in the contact pressure (from 0.115 MPa to 0.1572 MPa) experienced by the target takes place. The pressure values listed here are lower than their no-buffer case counterparts, demonstrating quantitatively the blast-wave-mitigation effects offered by the buffer.

Premature Deployment of the Air-vacated Buffer

In the case presented in this section, no virtual partition is placed between the ambient air and the buffer. Consequently, and due to a pressure discontinuity across the ambient-air/buffer interface, interaction between the ambient-air region and the buffer takes place before the arrival of the incident blast wave to the ambient-air/buffer interface. As will be discussed below, ambient-air/buffer interaction has a "shock-tube" effect which creates a forward-travelling blast wave within the buffer which precedes the transmitted blast wave caused by the interaction of the incident blast wave with the ambient-air/buffer interface. This condition can significantly lower the blast-wave-mitigation effect offered by the air-vacated buffer solution for at least two reasons: (a) the additional forward-travelling blast wave within the buffer provides increased loading onto the target structure; and (b) the static pressure within the buffer encountered by the incident blast wave is increased relative to the buffer initial pressure.

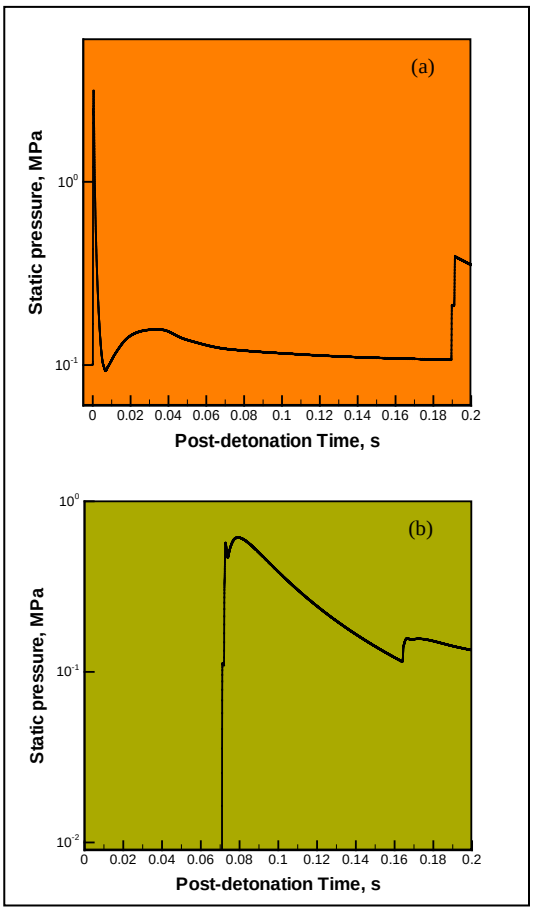

FIGURE 11. TEMPORAL EVOLUTION OF THE STATIC PRESSURE IN: (a) AN ELEMENT LOCATED NEAR THE EXPLOSIVE CHARGE; AND (b) AN ELEMENT ADJACENT TO THE RIGID, IMMOBILE TARGET STRUCTURE IN THE CASE WHEN AN AIR-VACATED BUFFER IS USED AND THE BUFFER IS ACTIVATED AT THE TIME OF ARRIVAL OF THE BLAST WAVE AT THE AMBIENT-AIR/BUFFER INTERFACE

Typical results obtained in this portion of the work are displayed in Figs. 12(a)-(b) and 13(a)-(b). In Figs. 12(a)-(b), spatial distribution of the static pressure through the Eulerian region at different post-detonation times are shown. In Figs. 13(a)-(b), temporal evolution of the static pressure is depicted for the same two elements defined earlier in conjunction with Figs. 9(a)-(b) and Figs. 11(a)-(b).

Examination of the results displayed in Figs. 12(a)-(b) reveals that: (a) interactions between ambient-air and the buffer occur before arrival of the detonation-induced decaying forward-travelling (incident) blast wave to the ambient-air/buffer interface. As a result of this interaction, a forward-travelling incident blast wave within the buffer and a backward-travelling release wave within the ambient-air region are generated. This behavior is analogous to the one normally observed in a shock tube in which the shock is generated by enabling the contact between the high pressure and ambient-air pressure sections of the tube. By Frame 30, it is seen that the incident "shock-tube" blast wave has already interacted with the rigid, immobile structure. As a consequence, a backward-travelling blast wave is created. Reflection of the shock-tube blast wave from the target structure increases the contact pressure on the structure from 0.0010 MPa to 0.6588 MPa; (b) by Frame 90, the detonation induced forward-travelling blast wave has completely passed through the backward-travelling release wave and has intersected with the backward-travelling reflected blast wave. As a result of this interaction, a new transmitted forward-travelling blast

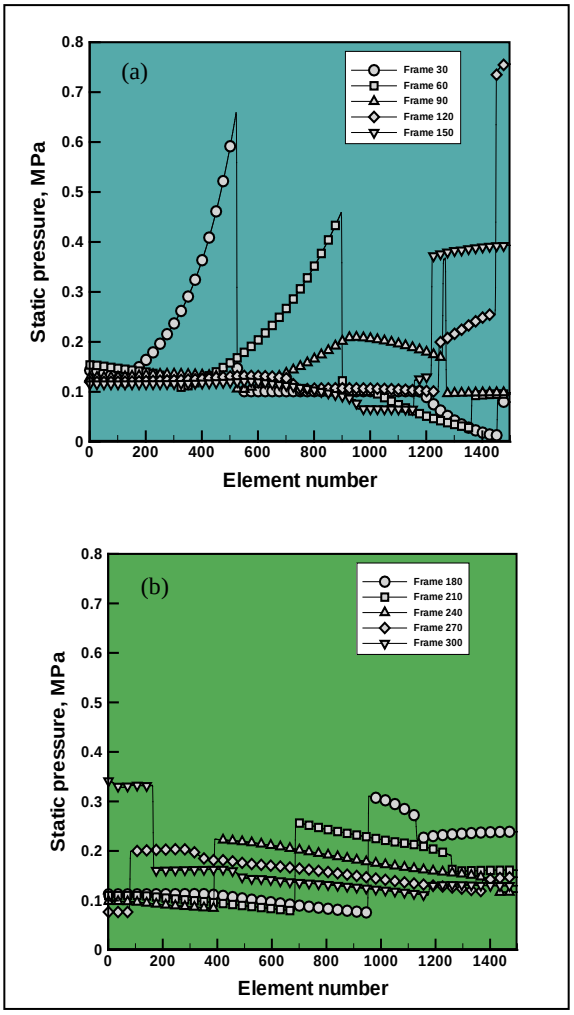

FIGURE 12 SPATIAL DISTRIBUTION OF THE DECAYING BLAST WAVE THROUGHOUT THE EULERIAN DOMAIN AS A FUNCTION OF THE POST-DETONATION TIME (QUANTIFIED BY THE ANIMATION- FRAME NUMBER) IN THE CASE WHEN AN AIR-VACATED BUFFER IS USED AND THE BUFFER IS ACTIVATED PRIOR TO THE ARRIVAL OF THE BLAST WAVE AT THE AMBIENT-AIR/BUFFER INTERFACE. THE FIGURE IS SEPARATED INTO PARTS (a) AND (b) TO IMPROVE CLARITY

wave is generated within (what used to be) the buffer region; (c) between Frames 110 and 120, the transmitted blast wave impacts the target structure causing its contact pressure to increase from 0.3191 MPa to 0.8288 MPa; (d) at Frame 120, one can see that a secondary forward-travelling incident blast wave has emerged, while the two reflected blast waves are travelling in the backward direction; (e) by Frame 180, it is seen that the two backward-travelling reflected blast waves have collapsed into a single one and that they have intersected with the secondary forward-travelling incident blast wave; and (f) between Frames 240 and 270, the secondary forward-travelling incident blast wave interacts with the target structure causing an increase in the contact pressure from 0.1078 MPa to 0.1484 MPa.

Examination of the results displayed in Figs. 13(a)-(b) reveals that: (a) temporal evolution of the pressure within the element adjacent to the detonation site is quite similar to those displayed in Figs. 9(a) and 11(a). In fact, the only significant differences occur again at times after the arrival of the reflected backward-travelling blast wave. This arrival causes an increase in the static pressure from 0.073 MPa to 0.4158 MPa. As expected, the pressure jump is seen to be higher than in the case of the timely-deployed air-buffer, Fig. 11(a). The lower value of the pressure in front of the backward-travelling reflected blast wave indicates that there is a release wave (travelling in the same direction) ahead of this blast wave; and (b) pressure experienced by the Eulerian element neighboring the target structure remains at the buffer pressure level until the arrival of the shock-tube incident blast wave. Reflection of this blast wave from the target structure (as well as reflection of the subsequent blast waves generated by the reflection of this wave from the ambient-air/buffer discontinuity) causes an increase in the contact pressure (to a nearly ambient-pressure value) experienced by the target structure. The arrival of the detonation-induced blast wave to the structure then causes a major increase (to a value of 0.8389 MPa) in the target structure contact pressure. Afterwards, the pressure decays exponentially and closely follows the pressure history previously observed in the case of Fig. 11(b). These observations clearly show that if the air-vacated buffer is deployed prematurely, its blast-wave-mitigation potential will be severely compromised. This topic is discussed in greater detail in the next section.

Blast-wave-mitigation Efficacy of the Air-vacated Buffer Concept

As mentioned earlier, the main purpose of the air-vacated buffer is to reduce blast-wave-induced loading onto the target structure. In the case of blast-wave-induced loading, it is a common practice to quantify the loading intensity using the maximum peak pressure experienced by the target structure and the maximum specific impulse (defined as an integral of the overpressure experienced by the target structure, integrated over time between the detonation time and the time of completion of the positive phase). Following this practice, the following two metrics are used to quantify the efficiency of air-vacated buffer rendered blast-wave-mitigation: (i) a ratio of the maximum peak pressure experienced by the target structure in a given case involving the use of a buffer

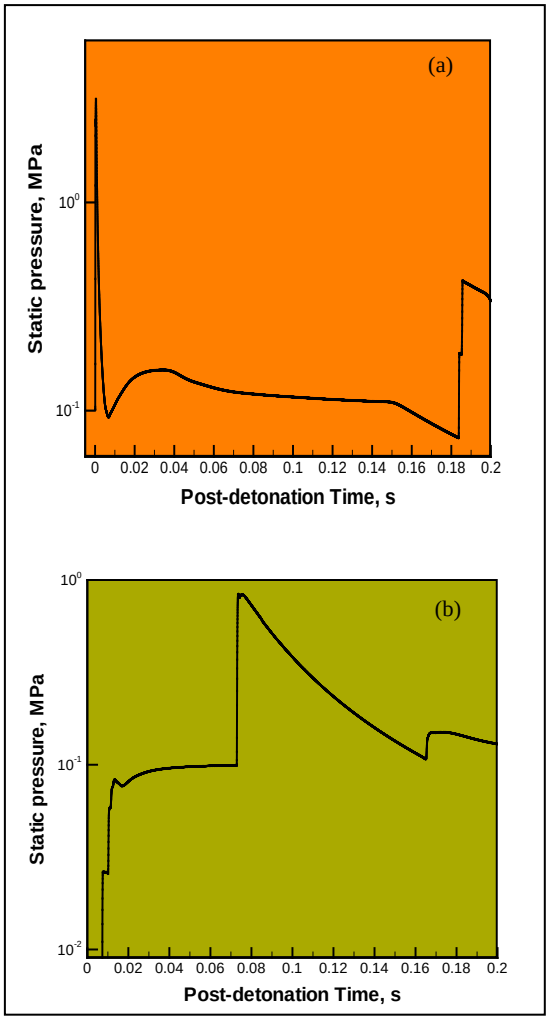

FIGURE 13 TEMPORAL EVOLUTION OF THE STATIC PRESSURE IN: (a) AN ELEMENT LOCATED NEAR THE EXPLOSIVE CHARGE; AND (b) AN ELEMENT ADJACENT TO THE RIGID, IMMOBILE TARGET STRUCTURE IN THE CASE WHEN AN AIR-VACATED BUFFER IS USED AND THE BUFFER IS ACTIVATED PRIOR TO THE ARRIVAL OF THE BLAST WAVE AT THE AMBIENT-AIR/BUFFER INTERFACE

and its counterpart in the case when no buffer is used; and (ii) a ratio of the maximum specific impulse experienced by the target structure in a given case involving the use of a buffer and its counterpart in the case when no buffer is used. Clearly, the smaller the values of the two metrics are, the more efficient is the buffer concept in mitigating the effect of blast-wave loading.

The results, such as those shown in Figs. 9(b), 11(b) and 13(b), can be used to compute the values of the two metrics for each specific case characterized by: (a) explosive charge energy/mass; (b) target/structure standoff distance; (c)buffer thickness; (d) buffer-material initial state (i.e. pressure, temperature, density, etc.); (e) ambient-air material state; and (f) the time of activation of the air-vacated buffer relative to the time of arrival of the incident blast wave to the ambient-air/buffer interface. As part of the present work, a detailed parametric study is carried out varying the aforementioned six (design) parameters over their respective physically acceptable and practically affordable ranges. Due to space limitations, detailed results obtained in this parametric study will not be presented here. Instead, a brief summary of the key findings obtained will be presented and discussed.

The results obtained mainly confirm the intuition: (i) that is, thicker buffers associated with a lower initial pressure/density are found to be more effective in mitigating the effect of blast wave loading; (ii) under the condition of constant values for the parameters (b)-(f), the buffer was found to be more effective in mitigating the effect of a weaker blast wave produced by the detonation of smaller explosive charges; (iii) at a given buffer thickness, there is a buffer-pressure threshold, i.e., a minimal buffer pressure below which no additional blast-wave-mitigation effects are obtained. The magnitude of the buffer-pressure threshold was found to decrease (and the associated blast-wave-mitigation effect to increase) with an increase in the buffer thickness. The buffer-pressure threshold was found to be related to the fact that when the transmitted blast wave within the buffer becomes quite weak in comparison to the detonation-induced blast wave the intensity of the former blast wave does not affect the blast-wave-mitigation efficacy of the buffer; and (iv) the time of deployment of the buffer relative to the arrival of the incident blast wave to the ambient-air/buffer interface plays a very critical role in the blast-wave-mitigation efficacy of the air-vacated buffer. That is, if the buffer is deployed prematurely, not only will the blast-mitigation efficiency of the buffer be compromised but also, under some circumstances the overall blast-wave loading experienced by the target structure may be increased relative to that observed in the no-buffer case. This finding is related to the aforementioned shock-tube effect.

Summary and Conclusions

Based on the results obtained in the present work, the following main summary remarks and conclusions can be drawn:

- Blast-wave-mitigation potential of an air-vacated buffer placed in front of the target structure is investigated computationally in the present work using advanced fluid-structure

interaction, non-linear dynamics, finite-element analyses.

- To verify and validate the employed computational methods and tools, it was first shown that they can quite accurately reproduce analytical solutions for a couple of well-defined blast-wave-propagation and interaction problems.
- Then the same methods and tools are used to analyze the detonation-induced blast wave generation, propagation and interaction with air/buffer and buffer/target-structure interfaces.
- The results obtained clearly revealed that significant blast-mitigation effects can be achieved through the use of the air-vacated buffer concept and that the extent of the blast-mitigation effect is a sensitive function of the buffer geometrical and vacated-air material-state parameters (e.g., pressure, mass density, etc.).
- In addition, it is found that, in order to fully exploit the air-vacated buffer concept, timely deployment of the buffer is very critical. Otherwise, the blast-wave-mitigation benefits offered by the air-vacated buffer may be severely compromised and, under certain conditions, adverse effects could result from use of the buffer.

REFERENCES

[1] M. Grujicic, H. Marvi, G. Arakere, W. C. Bell, I. Haque, "The Effect of Up-armoring the High-Mobility Multi-purpose Wheeled Vehicle (HMMWV) on the Off-road Vehicle Performance," Multidiscipline Modeling in Materials and Structures, 6, 2, 2010, 229–256.

[2] M. Grujicic, W. C. Bell, G. Arakere and I. Haque, "Finite Element Analysis of the Effect of Up-armoring on the Off-road Braking and Sharp-turn Performance of a High-Mobility Multi-purpose Wheeled Vehicle (HMMWV) ," Journal of Automobile Engineering, 223, D11, 2009, 1419–1434.

[3] M. Grujicic, G. Arakere, H. K. Nallagatla, W. C. Bell, I. Haque, "Computational Investigation of Blast Survivability and Off-road Performance of an Up-armored High-Mobility Multi-purpose Wheeled Vehicle (HMMWV) ," Journal of Automobile Engineering, 223, 2009, 301–325.

[4] M. Grujicic, G. Arakere, B. Pandurangan, W. C. Bell, T. He and X. Xie, "Material-modeling and Structural-mechanics Aspects of the Traumatic Brain Injury Problem," Multidiscipline Modeling in Materials and Structures, 6, 3, 2010, 335–363.

[5] M. Grujicic, W. C. Bell, B. Pandurangan and P. S. Glomski, "Fluid/Structure Interaction Computational Investigation of the Blast-Wave Mitigation Efficacy of the Advanced Combat Helmet," Journal of Materials Engineering and Performance, 20, 6, 2011, 877–893.

[6] F. G. Friedlander, "The wave equation on a curved space-time," Cambridge Monographs on Mathematical Physics, 2, Cambridge University Press, New York, 1976.

[7] P.W. Cooper, "Explosives engineering," New York: Wiley-VCH; 1996.

[8] D. Hyde, User's Guide for Microcomputer Programs, CONWEP and FUNPRO—Applications of TM 5-855-1, U.S. Army Engineer Waterways Experimental Station, Vicksburg, 1988.

[9] R. B. Bogoslovov, C. M. Roland and R. M. Gamache, "Impact-induced Glass-Transition in Elastomer Coatings," Applied Physics Letters, 90, 2007, 221910.

[10] M. Grujicic, B. Pandurangan, T. He, B. A. Cheeseman, C-F. Yen and C. L. Randow, "Computational Investigation of Impact Energy Absorption Capability of Polyurea Coatings via Deformation-Induced Glass Transition," Materials Science and Engineering A, 527, 2010, 7741-7751.

[11] M. F. Ashby, A. Evans, N. A. Fleck, L. J. Gibson, J. W. Hutchinson, and H. N. G. Wadley, "Metal Foams," Butterworth Heinemann, 2000.

[12] M. Grujicic, B. Pandurangan, W.C. Bell and S. Bagheri, "Shock-wave Attenuation and Energy-dissipation Potential of Granular Materials," Journal of Materials Engineering and Performance, 21, 2011, 167-179.

[13] J.W. Hutchinson and Z. Xue." Metal sandwich plates optimized for pressure impulses," International Journal of Mechanical Sciences, 47, 2005, 545–569.

[14] Srikanti Rupa Avasarala, "Blast Overpressure Relief Using Air Vacated Buffer Medium," M.S. Thesis, Massachusetts Institute of Technology, 2009.

[15] J.W. Tringe, J.D. Molitoris, and R.G. Garza et al, "Detailed comparison of blast effects in air and vacuum," UCRL-CONF 233223, American Physical Society, August 2007.

[16] D. Venable, R. W. Taylor, and B. T. Rogers et al, United States Patent 3804017, 1974.

[17] ABAQUS Version 6.10 EF1, User Documentation, Dassault Systems, 2010.

[18] L. Davison, Fundamentals of Shock Wave Propagation in Solids, Springer-Verlag, Berlin, Heidelberg, Germany, 2008.